

# Role of local disorder in the dielectric response of BaTaO<sub>2</sub>N

B. Ravel\*

*Biosciences Div, Argonne National Laboratory, Chicago, Illinois 20375, USA*

Y.-I. Kim and P. M. Woodward

*Department of Chemistry of Ohio State College of Mathematical and Physical Science, Ohio State University, Columbus, Ohio 43202, USA*

C. M. Fang

*Sciences Chimiques de Rennes, UMR 6226, CNRS-Université de Rennes, F-35042 Rennes, France*

(Received 9 February 2006; published 22 May 2006)

Short-range structural disorder of the high- $\kappa$  dielectric BaTaO<sub>2</sub>N is revealed by the analysis of the extended x-ray-absorption fine-structure (EXAFS) spectroscopy measured at the Ta  $L_{III}$  edge. Although previous neutron, x-ray, and electron diffraction studies have shown BaTaO<sub>2</sub>N to crystallize in a centrosymmetric, cubic structure, these EXAFS spectra show a wide distribution of first shell Ta-(O,N) distances with further implications to nonuniformity of the existing octahedral distortions. A distortion model based upon a density functional theory energy minimization for a  $4 \times 4 \times 4$  supercell of BaTaO<sub>2</sub>N was used to successfully interpret these EXAFS data. We find that structural distortions with very short correlation lengths exist in this material and that these distortions are consistent with the large dielectric permittivity of BaTaO<sub>2</sub>N.

DOI: [10.1103/PhysRevB.73.184121](https://doi.org/10.1103/PhysRevB.73.184121)

PACS number(s): 61.10.Ht, 77.22.Ch, 77.84.Bw, 77.84.Dy

## I. INTRODUCTION

A polar noncentrosymmetric arrangement of ions is taken as an essential factor for high dielectric permittivity ( $\kappa$ ) or ferroelectricity of crystals, where the permanent ionic dipoles will actively respond to the applied electric field.<sup>1</sup> Accordingly it has been elucidated that high- $\kappa$  ceramics exist only in the polar acentric crystals and the others with centric or nonpolar acentric point groups are unable to possess marked dielectric polarization. Recent studies on CaCu<sub>3</sub>Ti<sub>4</sub>O<sub>12</sub> (Ref. 2) and BaTaO<sub>2</sub>N,<sup>3</sup> however, present unexpected correlations between structure and dielectric property; while the crystal symmetries are described by centrosymmetric space groups; their dielectric constants are very high and nearly invariant with temperature. In the case of CaCu<sub>3</sub>Ti<sub>4</sub>O<sub>12</sub> with an  $Im\bar{3}$  space group, it was proposed that microstructures such as twin crystal boundaries<sup>4</sup> or barrier layers formed from surface defects<sup>5</sup> lead to the giant dielectric effect. For BaTaO<sub>2</sub>N, however, it is an open question whether the reported  $Pm\bar{3}m$  space group represents the local structure of its simple perovskite cube. The anion composition of BaTaO<sub>2</sub>N indicates that each octahedral Ta ion should be coordinated by four O<sup>2-</sup> and two N<sup>3-</sup> ions. With this nonequivalent coordination environment of [TaO<sub>4</sub>N<sub>2</sub>], a simple cubic unit cell of BaTaO<sub>2</sub>N can be achieved only when all the Ta<sup>+5</sup>-O<sup>2-</sup> and Ta<sup>+5</sup>-N<sup>3-</sup> bonding pairs have the same distance, which is very unlikely considering the distinct sizes and covalencies of O<sup>2-</sup> and N<sup>3-</sup> ions. A density functional theoretical calculation study supports this chemical intuition by showing that the lattice energy minima of BaTaO<sub>2</sub>N can be reached when the [TaO<sub>4</sub>N<sub>2</sub>] octahedra distort in a way that the point group symmetry is lowered from  $O_h$  (ignoring the distinction between oxide and nitride ions) to  $C_{4v}^6$ .<sup>6</sup> Therefore we presume that there can be structural distortions within BaTaO<sub>2</sub>N but with coherence lengths too small to be detected in the previ-

ous diffraction studies using x-ray,<sup>3</sup> neutron,<sup>7</sup> and electron<sup>3</sup> radiation sources. The possibility of local distortions should be investigated even though previous neutron diffraction work<sup>7</sup> did not find unusually large thermal factors for any of the sites.

Extended x-ray-absorption fine-structure (EXAFS) spectroscopy is well suited for examining possible local structural distortions in BaTaO<sub>2</sub>N. EXAFS is a local probe, sensitive to correlations on a length scale of a few Angstroms. Furthermore, the EXAFS measurement and its interpretation make no assumptions of symmetry or periodicity. Thus EXAFS can resolve local structural distortions which have very short correlation lengths and which might be missed in a Rietveld analysis of powder diffraction data. The data measured at the Ta  $L_{III}$  edge are of particular interest. Since the Ta cation lies at the center of the (O,N) octahedra of the BaTaO<sub>2</sub>N perovskite structure, these data will be especially sensitive to anionic displacements.

## II. SAMPLE PREPARATION AND MEASUREMENT

A fine powder ( $\sim 100$  nm) of BaTaO<sub>2</sub>N was prepared by ammonolysis,<sup>3</sup> dispersed within a quantity of boron nitride, and cold pressed into a pellet. Enough BaTaO<sub>2</sub>N powder was added for a transmission edge step of about 0.3 at the Ta  $L_{III}$  edge and enough boron nitride was used to make a pressed pellet of about  $\frac{1}{2}$  mm thickness. This sample is of an appropriate thickness for the EXAFS measurement,<sup>8</sup> is sufficiently uniform for high quality data collection,<sup>9</sup> and is rugged enough for manual handling and temperature cycling.

This sample was mounted on the cold finger of a Displex cryostat and EXAFS data were measured at 10, 100, 200, and 300 K at beamline X11B at the National Synchrotron Light Source. The unfocused, monochromatic beam was provided by a channel-cut Si(111) crystal. Adequate harmonic

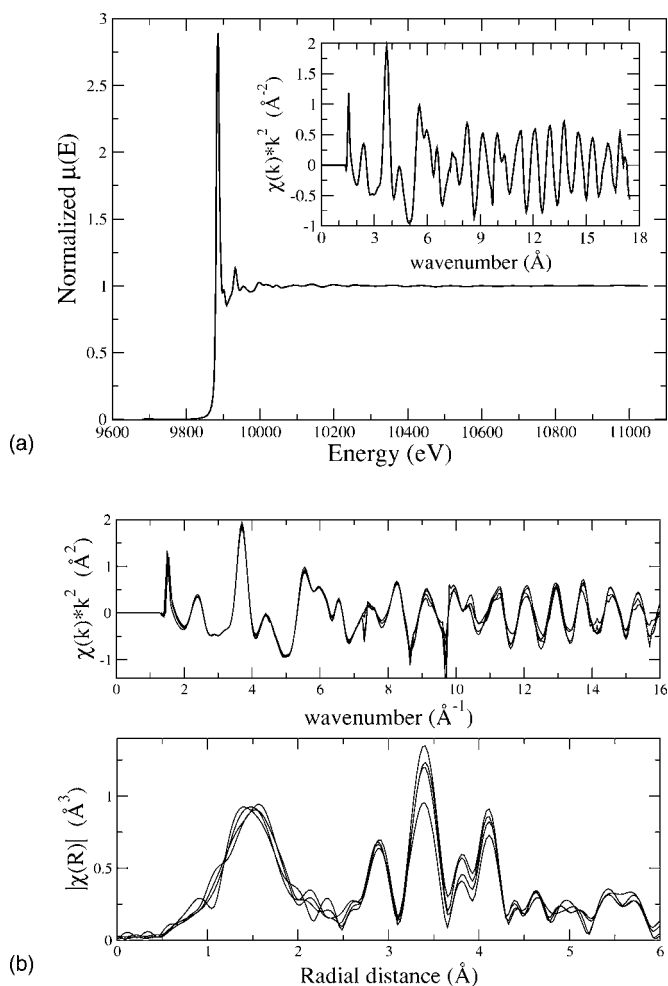


FIG. 1. (Top) Normalized  $\mu(E)$  and the extracted  $\chi(k)$  for BaTaO<sub>2</sub>N at 10 K. These data are the average of nine scans. (Bottom) Averaged data at 10, 100, 200, and 300 K as  $\chi(k)$  and  $|\bar{\chi}(R)|$ . The temperature dependence of the data is such that the amplitude of the signal diminished with temperature. The variability in the peak at about 1.5 Å is indicative of the difficulty of background removal in the presence of a strong white line, as discussed in Sec. VI.

rejection was accomplished by bending the second face of the crystal to attenuate the incident beam by about 40%. Incident and transmitted beam intensities were measured using ionization chambers filled with mixtures of Ar and N<sub>2</sub> and operated in a stable region of their I/V curves. Several scans were taken at each temperature and averaged. An example of the high quality of the data obtained is shown in Fig. 1.

The ATHENA program<sup>10,11</sup> was used to process the raw data. The AUTOBK<sup>12</sup> algorithm was used to fit a smoothly varying background function,  $\mu_0(E)$  to the data and to extract the oscillatory  $\chi(k)$  according to the formula

$$\mu(E) = \mu_0(E)[1 + \chi(E)], \quad (1)$$

where the photoelectron wave number  $k$  is related to the photon energy by  $k = \sqrt{2m_e(E - E_0)}/\hbar$  and  $E_0$  is the excitation energy ( $E_0 = 9881$  eV for Ta metal).

The ARTEMIS program<sup>10,11</sup> was used to analyze these data using the fitting models described below. Theoretical standards were computed using FEFF6 (Ref. 13) and used in the analysis.

### III. THE EXAFS FORMALISM

The theory is computed within a real-space, multiple-scattering framework.<sup>13</sup> The fine structure of the x-ray-absorption cross section is computed as a sum over all geometries by which an excited photoelectron can scatter from the atoms surrounding the absorber. For each scattering geometry  $\Gamma$  the following equation is evaluated:

$$\chi_{\Gamma}(k) = \frac{N_{\Gamma} S_0^2 F_{\Gamma}(k)}{2kR_{\Gamma}^2} e^{-2k^2\sigma_{\Gamma}} e^{-2R_{\Gamma}/\lambda(k)} \times \sin[2kR_{\Gamma} + \Phi_{\Gamma}(k) - 4k^3 C_{3,\Gamma}/3], \quad (2)$$

where  $R_{\Gamma} = R_{0,\Gamma} + \Delta R_{\Gamma}$ . Here, the terms  $F_{\Gamma}(k)$  and  $\Phi_{\Gamma}(k)$  are the scattering amplitude and phase shift for the path,  $\lambda(k)$  is the photoelectron mean free path, and  $R_{0,\Gamma}$  is the nominal length of the path as used in the computation. These terms are taken from the theory, FEFF6. The remaining terms are explained in the following paragraphs. Without the subscript  $\Gamma$ , Eq. (2) is the equation for single-scattering geometries. One significant feature of FEFF6 is that it computes an effective scattering function,<sup>14</sup>  $F_{\text{eff}}(k)$  and  $\Phi_{\text{eff}}(k)$ , for multiple scattering geometries. This effective scattering function replaces the  $F(k)$  and  $\Phi(k)$  terms of the single-scattering equation. Consequently, single- and multiple-scattering geometries can be treated with the same analytic formalism.

FEFF takes as its input data an initial configuration of atoms containing the absorbing atoms and the surrounding atoms that constitute its local environment. For the analysis presented herein, a cluster of atoms was determined using the perovskite structure known from crystallography.<sup>3</sup> FEFF computes all possible single-scattering (SS) and multiple-scattering (MS) geometries up to the seventh order of scattering and within a specified radius of the absorber. Thus the total  $\chi(k)$  function is obtained by taking the sum over all computed scattering paths

$$\chi(k) = \sum_{\Gamma} \chi_{\Gamma}(k), \quad (3)$$

where each  $\Gamma$  is a unique SS or MS scattering geometry, i.e., a path by which the photoelectron leaves its atom and scatter in sequence from one or more surrounding atoms. In a typical analysis problem, the spectrum is dominated by a relatively small number of short, single, and low-order multiple-scattering paths. Thus this possibly enormous summation is typically truncated to an easily managed number of terms.

The parametric terms in Eq. (2) which must be evaluated for each scattering path are  $N_{\Gamma}$ , the number of geometrically equivalent paths;  $S_0^2$ , a roughly constant intrinsic loss term used to account for the effect of the passive electrons during the photoexcitation of the deep core electron,<sup>15,16</sup>  $\Delta R$ , the variation in distance between absorber and scatterer compared to that used in the FEFF calculation;  $\sigma^2$ , the root mean

square variation in the distance between absorber and scatterer;  $E_0$ , an adjustment to the kinetic energy zero of the ejected photoelectron, and  $C_{3,\Gamma}$ , the third cumulant of the distribution,<sup>17</sup> which measures the anharmonicity of the distribution of distances between absorber and scatterer. These parametric terms are modified by the data analysis software to best fit the theoretical sum of paths in Eq. (3) to the measured data.

The analysis software used in this work is built on the IFEFFIT (Ref. 11) package, which has certain features which are particularly attractive for the analysis presented herein. Each of the parametric terms can be written as mathematical expressions which are functionally dependent upon more primitive fitting variables. Thus it is possible to build arbitrary constraints into a fitting model. The parametric terms for each path included in the fit can be related in ways that embody the underlying physics or chemistry of the analysis problem. This flexible approach to the EXAFS analysis problem is used to construct the fitting models described in Secs. IV and V.

#### IV. SIMPLE CUBIC PEROVSKITE MODEL

Since the crystallographic structure of BaTaO<sub>2</sub>N is that of a cubic perovskite, the undistorted cubic perovskite structure is a sensible starting point for our analysis of the EXAFS data. As we will see, this structural model is too simplistic to describe the measured data properly. Still, we will describe it in detail both to demonstrate that the measured EXAFS data indicate a complicated and distorted local structure in BaTaO<sub>2</sub>N and to justify the complexity of the fitting model described in Sec. V.

Theoretical fitting standards were computed using the  $Pm\bar{3}m$  structure<sup>3</sup> with  $a_0=4.113$  Å and Ba, Ta, and O at the (0,0,0),  $(\frac{1}{2}, \frac{1}{2}, \frac{1}{2})$ , and  $(\frac{1}{2}, \frac{1}{2}, 0)$  sites respectively. The subtle difference in the scattering power of the oxide and nitride ions was neglected. For each SS path used in this fitting model, the  $N_\Gamma$  term from Eq. (2) was set to the coordination number. The  $S_0^2$  parameter was fixed to a value of 0.928, the value computed for this material by full-multiple-scattering FEFF8 code. The fits were performed over the  $k$ -range 2–15.2 Å<sup>-1</sup> and the  $R$ -range 1–4.4 Å. A Kaiser-Bessel window with a sill width of 2 Å<sup>-1</sup> and simultaneous  $k$  weightings of 1 and 3 were used in the Fourier transforms during the fits.

The variable parameters used in the fit were an isotropic lattice expansion coefficient used to compute  $\Delta R$  for each path, an  $E_0$ , and  $\sigma^2$ 's for the first and fourth O coordination shells, the second Ba shell, and the third Ta shell. All multiple-scattering paths with half path lengths equal to or less than the distance to the third coordination shell were included in the fits. With one exception described below, no new fitting parameters were introduced with these MS paths. Their  $N_\Gamma$  parameters were set to the path degeneracies found by FEFF and the same  $E_0$  and  $S_0^2$  parameters were used for the MS paths as for the SS paths. The MS  $\Delta R$  parameters were also computed from the isotropic expansion coefficient. Finally, the  $\sigma^2$  parameters for the MS paths were computed from the SS  $\sigma^2$  following the scheme described in Ref. 18.

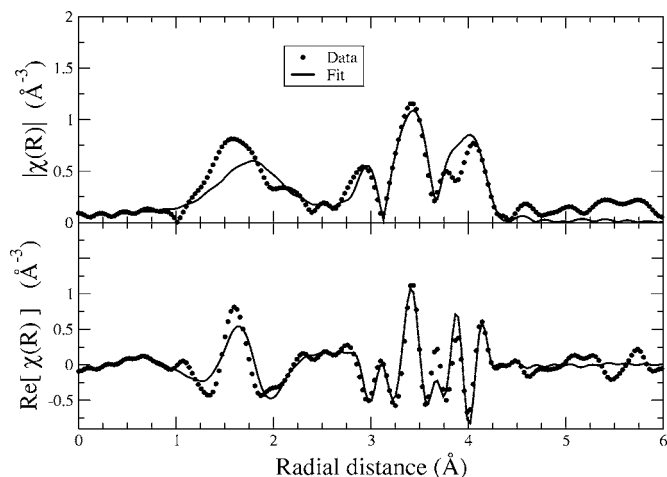


FIG. 2. Fit to the BaTaO<sub>2</sub>N data at 100 K using the cubic model. Note the significant misfits in the peak corresponding to the first coordination shell and in the regions between 3.5 and 3.9 Å.

Additional parameters were introduced in an attempt to improve the qualities of the fits. These included third cumulants of the absorber-scatterer distributions for each of the first three coordination shells and an additional  $E_0$  parameter applied separately to the MS paths with the same path length as the Ta third shell. Each of these parameters was statistically significant in the sense that they reduced the misfit to the data. They are discussed below.

An example of a fit using this model is shown in Fig. 2. Although this is the best fit obtained within the context of a purely cubic structural model, it is poor. There is a significant misfit in the first peak, which is dominated by the spectral weight of the first coordination shell. We also see a significant misfit in the region from 3.5 to 3.9 Å. The percentage misfit throughout the fitting range is around 15% for each measured temperature.

Along with the misfit, there are many indications among the fitting parameters, compiled in Table I, that this simple structural model is incomplete. The lattice expansion param-

TABLE I. Fitting parameters used in the cubic model. The values given for the  $\sigma^2$  parameters are the results of fitting the four temperatures to a single frequency (or Einstein) oscillator. The values for the remaining parameters are the averages of the four temperatures.

Parameter	Value
$\alpha$	0.024(5)
$E_0$	14.6(6) eV
$E_0(\text{MS})$	10.4(4) eV
$\sigma_{\text{O}}^2$	$\Theta=505(20)$ K, offset=0.0181(2) Å <sup>2</sup>
$\sigma_{\text{Ba}}^2$	$\Theta=261(45)$ K, offset=0.0065(6) Å <sup>2</sup>
$\sigma_{\text{Ta}}^2$	$\Theta=249(4)$ K, offset=0.0032(1) Å <sup>2</sup>
$\sigma_{\text{O4}}^2$	Very large
$C_3(\text{O})$	-0.0005(1) Å <sup>3</sup>
$C_3(\text{Ba})$	0.0008(2) Å <sup>3</sup>
$C_3(\text{Ta})$	0.0002(2) Å <sup>3</sup>

eter  $\alpha$  is around +2% at each temperature with no sensible dependence on temperature. The lattice parameter is well known at room temperature and certainly not larger at low temperature. As we see in Eq. (2), the distances and therefore the isotropic lattice expansion parameter is highly correlated to the quality of the scattering phases computed by FEFF. If there is a serious flaw in the structural model, this will translate into a serious flaw in the calculation of these phases. In this case, this has resulted in a spurious value for  $\alpha$ .

That the  $E_0$  parameter is quite large is a warning sign that this simple structural model inadequately describes the data. More troublesome is the fact the the fit was statistically improved by allowing some of the MS paths to have an independent  $E_0$ . This defies a physical interpretation and suggests the only role of the second  $E_0$  was to improve the fit quality in a statistical sense by compensating for something that was missing from the structural model. A similar argument can be made about each of the third cumulant parameters. The fit quality was improved, but the presence of nonzero third cumulants suggests that considerable structural disorder was absent from the model.

The  $\sigma^2$  values for each SS path at the four measured temperatures were fit to a single frequency (Einstein) oscillator model<sup>19</sup> with a static offset. The characteristic temperatures of oscillation from these fits are shown in Table I. The temperatures are reasonable numbers. The high characteristic temperature of the stiff Ta-O bond is typical of other perovskites,<sup>20,21</sup> as are the lower temperatures of the metal-metal bonds. The large static offsets are further evidence that this simple cubic structural model includes insufficient structural disorder compared to the real material.

These results taken together—the poor fit quality, the large static offsets to the  $\sigma^2$  values, the nonzero third cumulants, the large isotropic expansion coefficient, and the statistically significant second  $E_0$  parameter—require us to reject this fitting model if a better one can be found.

## V. LOCAL DISORDER MODEL

The total energy minimization performed by Fang *et al.*<sup>6</sup> was made starting with a box of atoms four unit cell lengths on a side. This box contained 64 unit cells or 320 atoms and used periodic boundary conditions. Starting with atoms at their nominal positions of high symmetry according to the  $Pm\bar{3}m$  crystal structure and with O and N atoms randomly distributed about the box, all atoms were allowed to relax in order to minimize the total energy of the configuration. This resulted in a highly disordered configuration. Our hope is that this disordered configuration addresses the shortcomings of the cubic perovskite model discussed in the previous section.

One approach to configurational data of this sort would be to evaluate Eq. (2) for each pair of atoms which includes a Ta atom as the absorber. The theoretical single-scattering contribution to the EXAFS would then be the properly normalized sum of the contributions of all such pairs of atoms. There is no conceptual reason not to approach the problem in this manner, however, the analysis software has certain hardware limitations which would be exceeded by the large

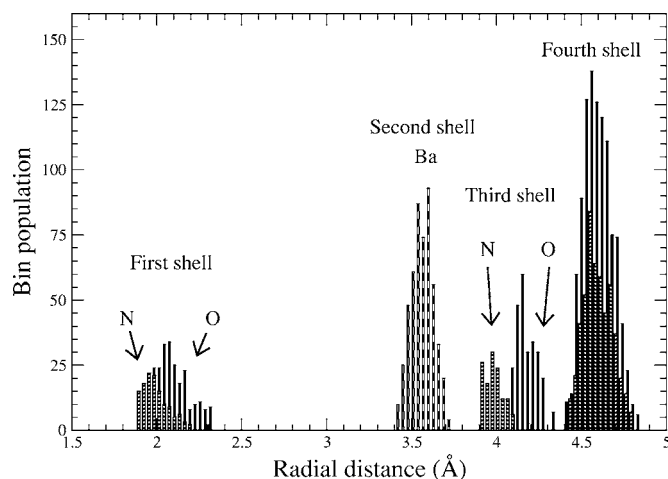


FIG. 3. Partial pair distribution functions from Ref. 6 divided into bins of 0.02 Å. Note that the SS path lengths involving O (solid bars) are generally longer than the path lengths involving N (short hash marks) in the first and third shells, but in the fourth shell the distributions of O and N scatterers overlap. The distribution of Ba atoms in the second shell (long hash marks) is nearly Gaussian.

number of absorber-scatterer pairs this straightforward approach would entail. This problem would get much worse when adding the multiple-scattering contributions to the analysis.

To accommodate this limitation in the analysis software, the SS paths were collected into bins of width 0.02 Å. Thus all SS paths with the same scatterer which were within 0.01 Å of the center of a bin were considered as a single path with the  $N_T$  term in Eq. (2) equal to the population of the bin. The histogram of SS paths is shown in Fig. 3. The O and N SS paths are gathered independently, as are the Ta-Ta SS paths which have O or N as the intervening atom. From this we see that the first coordination shell is bimodal, with an average Ta-N distance of 1.994 Å and an average Ta-O distance of 2.091 Å. This attraction of the N atom to the Ta atoms is seen also in the third coordination shell. The average Ta-Ta distance when the intervening atom is N is 3.985 Å while the average Ta-Ta distance with an intervening O atom is 4.179 Å. Interestingly, this bimodal character of the Ta-O and Ta-N partial pair distribution functions is not seen in the fourth coordination shell. This suggests that the correlation length of the distortions due to the relaxations of the O and N atoms is quite small. This would explain why significant local distortion is clearly seen in the EXAFS data (as discussed below) while the crystallography data<sup>3,7</sup> on BaTaO<sub>2</sub>N suggest the material maintains the  $Pm\bar{3}m$  symmetry of the simple perovskite structure.

As we saw in the simple cubic model and as has been observed in other perovskites,<sup>20,22</sup> the multiple-scattering contributions to the measured EXAFS cannot be neglected in the analysis. Again, we could simply solve Eq. (2) for each three atom group which includes a Ta atom as the absorber, but that would overwhelm the analysis software. So histograms were made, grouping together similar paths. This grouping is, however, more subtle for three-atom groups due to the effect of the scattering angle on the contribution from

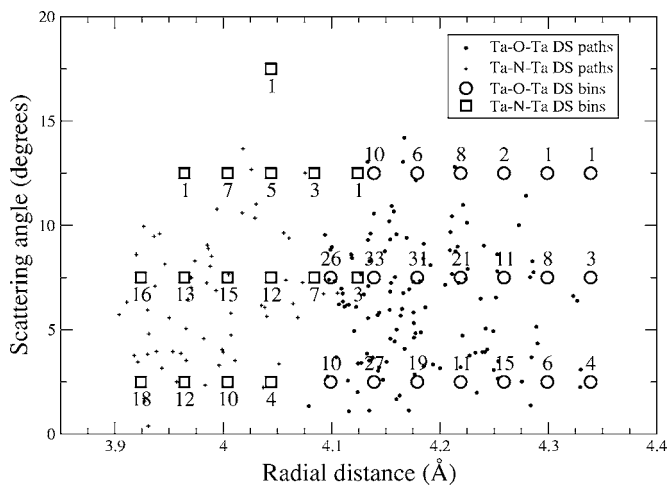


FIG. 4. Distribution in path lengths and scattering angles of double-scattering (DS) Ta-O-Ta (dots) and Ta-N-Ta (crosses) paths from Ref. 6. Also shown are the  $5^\circ \times 0.03 \text{ \AA}$  bins used to represent the DS paths with O (circles) and N (squares) in the analysis. The labels represent the number of paths in each bin.

a three-atom path. In general, the scattering amplitude is strongly peaked in the forward and backward directions and this amplitude diminishes strongly with angle away from  $0^\circ$  or  $180^\circ$ .<sup>13,23</sup> The scattering phase shift also is strongly dependent on angle.

All three-atom groups involving first shell Ta and the intervening O or N atoms were extracted from the energy-minimized box of atoms. The distribution of length and scattering angles for all such double-scattering paths is shown in Fig. 4. Again this distribution is bimodal in distance (but, interestingly, not in angles), with the N-containing paths being the shorter. These paths are collected into bins of size  $5^\circ$  by  $0.03 \text{ \AA}$ . The number of paths in each bin is shown next to the bin position.

For use with the single-scattering histograms, FEFF6 was run using the same  $Pm\bar{3}m$  structure used in the cubic model. The O or N first shell SS path was used for the amplitudes and phases of each O or N bin. Similarly, the Ba and Ta SS paths were used for each of those bins. The difference between each bin position and the distance used in the FEFF calculation was applied to Eq. (2) as a static  $\Delta R$  correction.

That simple trick was not possible for the MS paths. The scattering amplitudes  $F_T(k)$  and phase shifts  $\Phi_T(k)$  are quite sensitive to scattering angles and there is no simple parametrization of that angular dependence in Eq. (2). Consequently, specialized input to the FEFF program was prepared to compute each bin shown in Fig. 4 individually. The Ta-O-Ta and Ta-N-Ta configurations shown in Fig. 4 were used to compute those double- and triple-scattering contributions. A similar histogram was made for all O/N-Ta-O/N three-atom configurations and FEFF was run to generate those double and triple scattering contributions. For this latter histogram, O and N were treated as indistinguishable. This is a reasonable approximation since O and N differ by only 1 electron and so have very similar scattering functions.

In total, 79 SS bins were used in the fits along with 138 nearly collinear DS and TS bins. Binning the various SS and

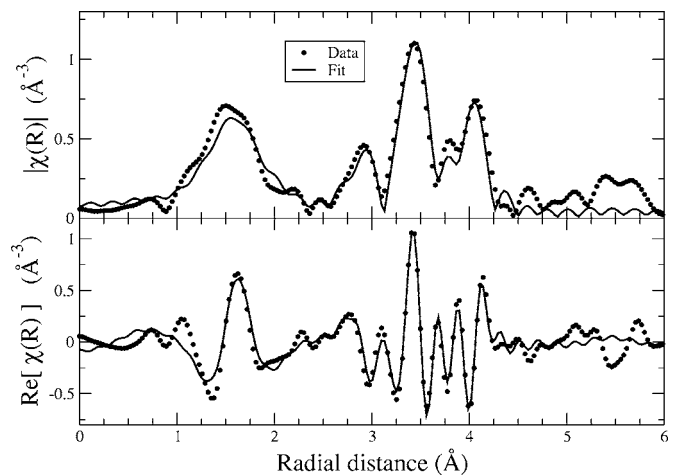


FIG. 5. Fit to the BaTaO<sub>2</sub>N data at 100 K using the local disorder model.

MS contributions in this manner made the problem of modeling the disorder predicted by the energy minimization model tractable for the analysis software.

It is important to keep in mind that this fitting model introduces several sources of systematic error: (1) the use of a single calculated scattering function for all SS bins of an atomic species, (2) the bundling of the MS paths into bins which subtend a rather large range of angles, and (3) the lack of a convenient way to parametrize the details of the distributions of atoms and therefore the lack of a way to modify these distributions during the fit. Despite these sources of error, this fitting model describes the data much better than the simpler cubic model both in terms of the fit quality and ability to interpret the physical meaning of the fitting parameters.

This structural model accommodates only a few reasonable fitting parameters. The same value for  $S_0^2=0.928$  was used as in the cubic perovskite model. An isotropic expansion coefficient is used, as is a single  $E_0$  parameter. A  $\sigma^2$  is used for each SS histogram and, hopefully, can be interpreted as a purely thermal disorder. The possibility that the  $\sigma^2$ 's for the first shell N histogram and the third shell Ta histogram with a N interceding atom might be different from the corresponding O  $\sigma^2$ 's was considered. Allowing an independent first shell N  $\sigma^2$  did not improve the fit and so cannot be independently measured. The  $\sigma^2$  for third shell Ta with an interceding N did improve the fit. The  $\sigma^2$ 's for the MS bins were computed from the SS  $\sigma^2$ 's using the same scheme used for the cubic model. Third cumulant parameters were not needed as a significant disorder was inherent to the structural model.

These fits were performed over the  $k$ -range  $3-15.5 \text{ \AA}^{-1}$  and the  $R$ -range  $1.2-4.5 \text{ \AA}$ . A Kaiser-Bessel window with a sill width of  $2 \text{ \AA}^{-1}$  and simultaneous  $k$  weightings of 1 and 3 were used in the Fourier transforms during the fits.

An example of this fit is shown in Fig. 5 and the results of the fit are given in Table II. This fit is still not exceptionally good—percentage misfits are between 5% and 9% at the different temperatures using this model. But that represents a significant improvement over the simpler model. The first

TABLE II. Fitting parameters used in the disordered model. The values given for the  $\sigma^2$  parameters are the results of fitting the four temperatures to a single frequency (or Einstein) oscillator. The values for the remaining parameters are the averages of the four temperatures.

Parameter	Value
$\alpha$	0.0034(5)
$E_0$	10.2(1) eV
$\sigma_{\text{O}}^2$	$\Theta=441(85)$ K, offset=0.0039(12) $\text{\AA}^2$
$\sigma_{\text{Ba}}^2$	$\Theta=249(25)$ K, offset=0.0010(3) $\text{\AA}^2$
$\sigma_{\text{TaO}}^2$	$\Theta=302(42)$ K, offset=-0.0008(3) $\text{\AA}^2$
$\sigma_{\text{TaN}}^2$	$\Theta=577(89)$ K, offset=-0.0026(7) $\text{\AA}^2$
$\sigma_{\text{O4}}^2$	$\Theta=343(39)$ K, offset=0.0051(12) $\text{\AA}^2$

peak is still a huge source of the misfit, but the bimodal distribution of scatterers is a significant improvement over the cumulant distribution used in the previous fit. This result is unsurprising—it is well established<sup>24</sup> that the cumulant expansion is only useful in EXAFS in situations where the distribution is only slightly anharmonic.

Even more significant is the improvement of the fit in the region from 3.5 to 3.9  $\text{\AA}$  compared to the fit with the cubic perovskite model. The structural disorder is very apparent in this region which includes the contributions of the many different nearly collinear-multiple scattering paths. This superposition of paths with subtle phase relationships is essential to fitting this portion of the spectrum and was completely lacking in the cubic model.

The fit to the cubic model required the addition of several parameters which were difficult to interpret, including large third cumulants and a second  $E_0$  shift. In light of the success of the local disorder model, it is clear that these additional parameters served as an arbitrary compensation for the missing disorder and approximated the effect of the angular distribution of the MS paths on the phase of the fitted function.

The values for the fitting parameters are given in Table II.  $\alpha$  is quite small and  $E_0$  is not unreasonably large. Again, the  $\sigma^2$  values at the four temperatures were fit to a single frequency (Einstein) oscillator model<sup>19</sup> and the characteristic temperature, and static offset is given in the table. The isotropic expansion parameter is much smaller than for the other model, although not consistent with zero as might be expected. The characteristic temperatures for the various bonds are mostly reasonable. The first shell bond is quite stiff, as expected from the limited variation in the first shell peak seen in the bottom of Fig. 1. Even the fourth shell oxygen  $\sigma^2$  was well defined in this fitting model. That the static offsets in the single frequency oscillator fits are generally much smaller in this model is unsurprising given that a significant level of static disorder is included *a priori* in this model.

## VI. DISCUSSION

We emphasize that this analysis is not a *solution* to the local structure of BaTaO<sub>2</sub>N. Instead it is an indication of the

extent to which the theoretical results of Fang *et al.* in Ref. 6 are consistent with the measured data. To the extent that the approximations made in constructing the histogram representation of the scattering theory are reasonable, the results of Fang *et al.* are a good, but incomplete, description of the data.

The main shortcoming of the structural model is that it seems to include slightly too little disorder in the partial pair distribution functions for most of the elements. Were the level of disorder accurate, one would expect a static offset consistent with zero for each of the fits to a single frequency oscillator. That would mean that each  $\sigma^2$  was a measure only of the thermal portion of the disorder in the partial pair distribution functions and that the static component of the disorder was completely accounted for by the energy minimization of the structure. This discrepancy may also be the result of the approximations made in constructing the histograms.

On the other hand, there were some limitations to these data. The presence of the white line in the raw data (see Fig. 1) combined with the relatively short Ta-N distance means that the problem of background removal is quite severe. The parameters used to determine the background function in Eq. (1) are highly correlated to the fitting parameters which affect the low- $R$  Fourier components of the data.<sup>12</sup> The practical consequence of this is that the data were unable to support separate  $\sigma^2$  parameters for O and N components of the first coordination shell. The failure to determine completely the structural disorder in the low- $R$  region and, indeed, the extent to which the data are poorly fit in the low- $R$  region cannot be blamed only on the deficiencies of the structural model. The data shown in Fig. 1, excellent as they are, simply do not support a better determination of the structure.

Despite the difficulties in modeling the local structural complexity of BaTaO<sub>2</sub>N, this Ta  $L_{III}$  edge EXAFS analysis delivers enough qualitative information on the Ta local structure to explain the observed dielectric behavior. Wide dispersion of the first shell Ta-(O,N) distances indicates the asymmetric coordination around Ta and also the stochastic O/N distribution over the octahedral corners. This combined with the absence of superstructure peaks in the diffraction patterns indicates that the distortion of the BaTaO<sub>2</sub>N lattice occurs with no regularity or periodicity. In the well-relaxed geometry described above, Ta ions will favor the octahedral distortions to maximize electrostatic stabilizations, certainly developing local polarizations. The failure to find uniform shapes of Ta-(O,N)<sub>6</sub> octahedra implies that the various octahedral configurations have continuously changing energies with minute differences. Interestingly in the Rietveld refinement of the x-ray or neutron diffraction data, the atomic displacement parameters were reasonably small<sup>7</sup> with the diffraction peak widths comparable to those of well-crystallized ceramics. This indirectly demonstrates both the sensitivity of the EXAFS technique and that the heavier components, Ba and Ta, remain very close to the ideal symmetry positions. It is worth noting that the Ba framework, a simple cubic lattice with the edge length of 4.113  $\text{\AA}$  at 295 K, does not undergo a discernible distortion. Thus all the Ta ions are provided with oversized spaces in which they can shift. With the structural features discussed above—flexibility of Ta-(O,N) bond distances, nonzero polar momentum within Ta-(O,N)<sub>6</sub> octa-

hedra, a large volume for the Ta motion, and highly polarizable component ions—BaTaO<sub>2</sub>N can show a large dielectric response to the applied field with high  $\kappa$ . However the random nature of the lattice distortion seems to suppress cooperative switching in either the electric polarization or the atomic displacements.

It is interesting to note that the calculations<sup>6</sup> predict the Ta-N bonds to be shorter on average than the Ta-O bonds. On the one hand such a trend might be expected if the Ta-N bonds are more covalent than the Ta-O bonds, but this trend runs counter to expectations based on ionic radii. To illustrate this consider<sup>25</sup> that the cubic-cell edge of BaTaO<sub>2</sub>N is 4.113 Å, which is larger than the value of 3.988 Å seen for KTaO<sub>3</sub>, despite the fact that the K<sup>+</sup> ion is slightly larger than the Ba<sup>2+</sup> ion. However, the larger cell edge seen in BaTaO<sub>2</sub>N can be, in part, attributed to the presence of locally distorted octahedra, which are known to take a larger volume than comparable symmetric octahedra according to the distortion theorem.<sup>26</sup> The relative lengths of M-O and M-N bonds in oxynitride perovskites is a question that merits further study. We note that, while this work confirms the presence of the

locally distorted octahedra predicted by the calculations, we cannot distinguish between oxide and nitride ions in the EXAFS analysis.

To close, this work suggests a very enticing possibility for future study. The EXAFS data could be tied much more closely to the determination of the minimum energy structure. One could imagine evaluating Eqs. (2) and (3) during the course of the energy minimization. At every step in the energy minimization, the theoretical EXAFS could be evaluated and compared to the data. An  $\mathcal{R}$  factor from the fit could be used as an entropy term in the energy minimization. In this way, the quality of fit to the EXAFS data could be part of the energy budget driving the structural solution.

#### ACKNOWLEDGMENTS

Y.I.K. and P.M.W. acknowledge funding from the Center for the Design of Materials, which is supported by the National Science Foundation (Grant No. CHE-043567). C.M.F. acknowledges G. de Wijs for helpful discussion.

---

\*Electronic address: bravel@anl.gov; URL: <http://cars9.uchicago.edu/~bravel>

- <sup>1</sup>M. Lines and A. Glass, *Principles and Applications of Ferroelectrics and Related Materials* (Oxford, New York, 1997).
- <sup>2</sup>M. Subramanian, D. Li, N. Duan, B. Reisner, and A. Sleight, *J. Solid State Chem.* **151**, 323 (2000).
- <sup>3</sup>Y.-I. Kim, P. Woodward, K. Baba-Kishi, and C.-W. Tai, *Chem. Mater.* **16**, 1267 (2004).
- <sup>4</sup>M. Subramanian and A. Sleight, *Solid State Sci.* **4**, 347 (2002).
- <sup>5</sup>D. Sinclair, T. Adams, F. Morrison, and A. West, *Appl. Phys. Lett.* **80**, 2153 (2002).
- <sup>6</sup>C. Fang, G. de Wijs, E. Orhan, G. de With, R. de Groot, H. Hintzen, and R. Marchand, *J. Phys. Chem. Solids* **64**, 281 (2003).
- <sup>7</sup>F. Pors, R. Marchand, Y. Laurent, P. Batcher, and G. Roullet, *Mater. Res. Bull.* **23**, 1447 (1988).
- <sup>8</sup>E. A. Stern and K. Kim, *Phys. Rev. B* **23**, 3781 (1981).
- <sup>9</sup>K. Q. Lu and E. A. Stern, *Nucl. Instrum. Methods Phys. Res.* **212**, 475 (1983).
- <sup>10</sup>B. Ravel and M. Newville, *J. Synchrotron Radiat.* **12**, 537 (2005).
- <sup>11</sup>M. Newville, *J. Synchrotron Radiat.* **8**, 322 (2001).
- <sup>12</sup>M. Newville, P. Liviš, Y. Yacoby, J. J. Rehr, and E. A. Stern, *Phys. Rev. B* **47**, 14126 (1993).

- <sup>13</sup>S. I. Zabinsky, J. J. Rehr, A. Ankudinov, R. C. Albers, and M. J. Eller, *Phys. Rev. B* **52**, 2995 (1995).
- <sup>14</sup>J. J. Rehr and R. C. Albers, *Phys. Rev. B* **41**, 8139 (1990).
- <sup>15</sup>E. A. Stern and S. M. Heald, in *Handbook of Synchrotron Radiation*, edited by E. E. Koch (North-Holland, New York, 1983), Chap. 10, pp. 995–1014.
- <sup>16</sup>G. G. Li, F. Bridges, and C. Booth, *Phys. Rev. B* **52**, 6332 (1995).
- <sup>17</sup>G. Bunker, *Nucl. Instrum. Methods Phys. Res.* **207**, 437 (1983).
- <sup>18</sup>E. Hudson, P. G. Allen, L. J. Terminello, M. A. Denecke, and T. Reich, *Phys. Rev. B* **54**, 156 (1996).
- <sup>19</sup>E. Sevillano, H. Meuth, and J. J. Rehr, *Phys. Rev. B* **20**, 4908 (1979).
- <sup>20</sup>B. Ravel, E. A. Stern, R. I. Vedrinskii, and V. Kraizman, *Ferroelectrics* **206–207**, 407 (1998).
- <sup>21</sup>N. Sicron, B. Ravel, Y. Yacoby, A. E. Stern, F. Dogan, and J. Rehr, *Phys. Rev. B* **50**, 13168 (1994).
- <sup>22</sup>O. Hanske-Petitpierre, Y. Yacoby, J. Mustre de Leon, E. A. Stern, and J. J. Rehr, *Phys. Rev. B* **44**, 6700 (1991).
- <sup>23</sup>P. A. Lee and J. B. Pendry, *Phys. Rev. B* **11**, 2795 (1975).
- <sup>24</sup>P. D'Angelo, A. Di Nola, A. Filipponi, N. Pavel, and D. Roccatano, *J. Chem. Phys.* **100**, 985 (1994).
- <sup>25</sup>E. Zhurova, Y. Ivanov, V. Zavodnik, and V. Tsirel'son, *Acta Crystallogr., Sect. B: Struct. Sci.* **56**, 594 (2000).
- <sup>26</sup>I. Brown, *Acta Crystallogr., Sect. B: Struct. Sci.* **48**, 553 (1992).